from conductors and enhanced linear media, IEEE Trans Microwave Theory Tech 47 (1999), 2075–2084.
3. D.R. Smith, W.J. Padilla, D.C. Vier, S.C. Nemat-Nasser, and S. Schultz, Composite medium with simultaneously negative permeability and permittivity, Phy Rev Lett 84 (2000), 4184–4187.
4. R.A. Shelby, D.R. Smith, and S. Schultz, Experimental verifications of a negative index of refraction, Science 292 (2001), 77–79.
5. R.W. Ziolkowski, Design fabrication and testing of double negative metamaterials, IEEE Trans Antennas Propag 51 (2002), 1516–1529.
6. L. Wu, S. He, and L. Shen, Band structure for one-dimensional photonic crystal containing left-handed materials, Phy Rev Lett B 67 (2003), 235103.
7. M. Bayindir, K. Aydin, E. Ozbay, P. Markes, and C.M. Soukoulise, Transmission properties of composites metamaterials in free space, Appl Phy Lett 81(2002), 120–122.
8. H. Cory and C. Zach, Wave propagation in metamaterials multilayered structure, Microwave Opt Technol Lett 40 (2004), 460.
9. C. Caloz and T. Itoh, Novel microwave devices and structures based on the transmission line approach of meta-materials, IEEE Inter Microwave Symp Dig (2003) 195–198.
10. D. Hrabar, J. Bartolic, and Z. Sipus, Waveguide miniaturization using uniaxial negative permeability metamaterials, IEEE Trans Antennas Propag 53 (2005), 110–119.
11. K. Aydin, K. Guven, M. Kafesaki, L. Zhang, and C.M. Soukoulis, E. Ozbay, Experimental observation of true left-handed transmission peaks in metamaterial, Opt Lett 29 (2004), 2623.
12. J. Gerardin and A. Lakhtakia, Negative index of refraction and distributed bragg reflectors, Microwave Opt Technol Lett 34 (2002), 409–411.
13. R. Ruppin, Bragg reflectors containing left-handed materials, Microwave Opt Technol Lett 38 (2003), 494, 495.
14. I. Nefedov and S. Atretyakov, Photonic band gap structure containing metamaterials with negative permittivity and permeability, Phy Rev Lett E 66 (2002) 036611.
15. I.V. Shadrivov, A.A. Sukhoukove, and Y.S. Kivshar, Complete band gaps in one-dimensional left-handed periodic structures, Phy Rev Lett 95 (2005), 193903.1–193903.4.
16. N. Engheta, An idea for thin subwavelength cavity resonators using metamaterials with negative permittivity and permeability," IEEE Antennas Wireless Propag Lett 1 (2002), 10–13.
17. A.S. Saleh and H. Aubert, Self-similar multi-slab media with variable lacunarity for the design of microwave filters, Electron Lett 37 (2001), 1071–1073.
18. A.S. Saleh and H. Aubert, Use of variable lacunarity, multi-gap, Cantor slabs in waveguides for the design of microwave filters, Microwave Opt Technol Lett 28 (2001), 127–130.
19. D.L. Jaggard and X. Sun, Reflection from fractal multilayers, Opt Lett 15 (1990), 1428–1430.
20. A.D. Jaggard and D.L. Jaggard, Scattering from fractal superlattices with variable lacunarity, J Opt Soc Am A 15 (1998), 1626–1635.

A NOVEL CONCEPT FOR RECONFIGURABLE FREQUENCY SELECTIVE SURFACES BASED ON SILICON SWITCHES

Xiaotao Liang,[1] Douglas H. Werner,[1] and Brian Weiner[2]
[1]Department of Electrical Engineering
The Pennsylvania State University
University Park, PA 16802
[2]Department of Physics
The Pennsylvania State University
University Park, PA 16802

Received 24 May 2006

ABSTRACT: *The authors describe a novel concept for reconfigurable frequency selective surfaces based on metallic dipole and cross-dipole elements connected by switches on an exposed silicon substrate. As the conductivity of silicon can be varied over a large dynamic range by photonic excitation, it represents a good candidate substrate material for producing effective switches. The genetic algorithm was used to obtain optimal performance of the switch with respect to variations of the geometric and electrical parameters of the design for desired excitation frequencies.* © 2006 Wiley Periodicals, Inc. Microwave Opt Technol Lett 49: 109–114, 2007; Published online in Wiley InterScience (www.interscience.wiley.com). DOI 10.1002/mop.22041

Key words: *frequency selected surface; reconfigurable silicon; genetic algorithm*

1. INTRODUCTION

There has been a significant amount of interest in frequency selective surfaces (FSSs) in recent years for a variety of applications, such as electromagnetic filtering devices for reflector antenna systems, radomes, absorbers, and artificial electromagnetic bandgap materials [1]. A typical FSS is comprised of one or more screens, which have two-dimensional (2D) periodic patterns generated by a unit cell containing either metallic patches or apertures. Each of the FSS screens is backed by a thin dielectric slab. When exposed to electromagnetic radiation, the periodic metallic features resonate at certain frequencies depending upon the dielectric properties of the substrate and the geometry of the unit cell. In electromagnetic filtering applications formed with strip dipole metallic elements the response spectra for the FSS exhibits a strong stopband at resonance, where the wavelength is approximately twice the length of the dipoles. A new reconfigurable FSS design concept was introduced in Refs. 2 and 3 that was based on a periodic array of fixed metallic linear or cross-dipole elements interconnected by a matrix of independently addressable switches. The FSS could be reconfigured by turning switches "ON" or "OFF" and thus changing the filter response of the device. The unit cell that generates this reconfigurable frequency selective surface (RFSS) is comprised of an 8 by 8 array of linear dipoles connected by ideal switches as shown in Figure 1(a). To demonstrate the flexibility of this RFSS concept, the switch settings were optimized using a genetic algorithm (GA) to produce two stopbands at 4.5 and 7 GHz [3]. Figure 1(b) shows the response spectra associated with these designated stopbands. In this article we discuss another type of FSS design, shown in Figure 2(a), which is composed of metallic cross-dipole elements connected by switches. As in the previous example, the GA is used to determine the optimal switch settings for the RFSS and produces a dual-band response shown in Figure 2(b).

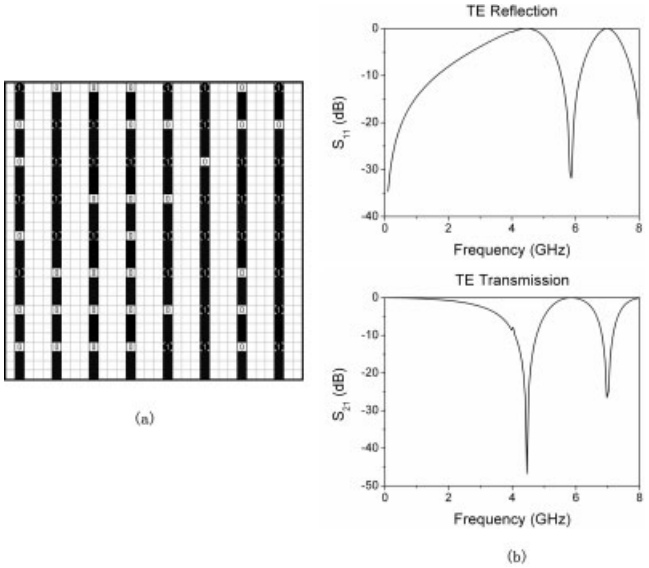

Figure 1 (a) A dipole RFSS geometry with GA optimized switch settings "1 " indicates the switch is closed and a "0 " indicates the switch is open; (b) frequency response (transmission and reflection) for the FSS is shown in (a)

2. SILICON SWITCHES

It is particularly attractive to consider RFSSs based on silicon as the conductivity of this material varies in response to the intensity of applied light sources. This variation can be explained in terms of the production of a plasma layer at the surface of the silicon switches, which can be produced by an intense light source such as a laser. This layer contains free charges, which alter the refractive index of the plasma region and thus the conductivity. It is possible to analyze the refractive index of this region in terms of classical electron-hole plasma theory. Moreover, by taking into account the contribution of bound charges using the static dielectric constant of the host lattice in place of the dielectric constant of free space, one can use Drude theory to predict the behavior of the conductivity [4].

The real and imaginary parts of the permittivity ε_r of silicon are calculated using

$$\varepsilon_r = \varepsilon_L - \frac{\omega_p^2}{\omega^2 + \nu^2} - j\frac{\nu}{\omega}\frac{\omega_p^2}{\omega^2 + \nu^2}, \tag{1}$$

where the permittivity of silicon has a value of $\varepsilon_L = 11.8$. The last two terms of Eq. (1) can be expressed as

$$\frac{\omega_p^2}{\omega^2 + \nu^2} = \frac{ne^2}{\varepsilon_0 m^*}\frac{\tau^2}{1 + \omega^2\tau^2} = \frac{n_{p0}e^2\tau_p^2}{m_p^*\varepsilon_0(1 + \omega^2\tau_p^2)} + \frac{n_p e^2\tau_p^2}{m_p^*\varepsilon_0(1 + \omega^2\tau_p^2)} + \frac{n_e e^2\tau_e^2}{m_e^*\varepsilon_0(1 + \omega^2\tau_e^2)}, \tag{2a}$$

$$\frac{\nu}{\omega}\frac{\omega_p^2}{\omega^2 + \nu^2} = \frac{ne^2}{\varepsilon_0 m^*\omega}\frac{\tau}{1 + \omega^2\tau^2} = \frac{n_{p0}e^2\tau_p}{\omega m_p^*\varepsilon_0(1 + \omega^2\tau_p^2)} + \frac{n_p e^2\tau_p}{\omega m_p^*\varepsilon_0(1 + \omega^2\tau_p^2)} + \frac{n_e e^2\tau_e}{\omega m_e^*\varepsilon_0(1 + \omega^2\tau_e^2)}, \tag{2b}$$

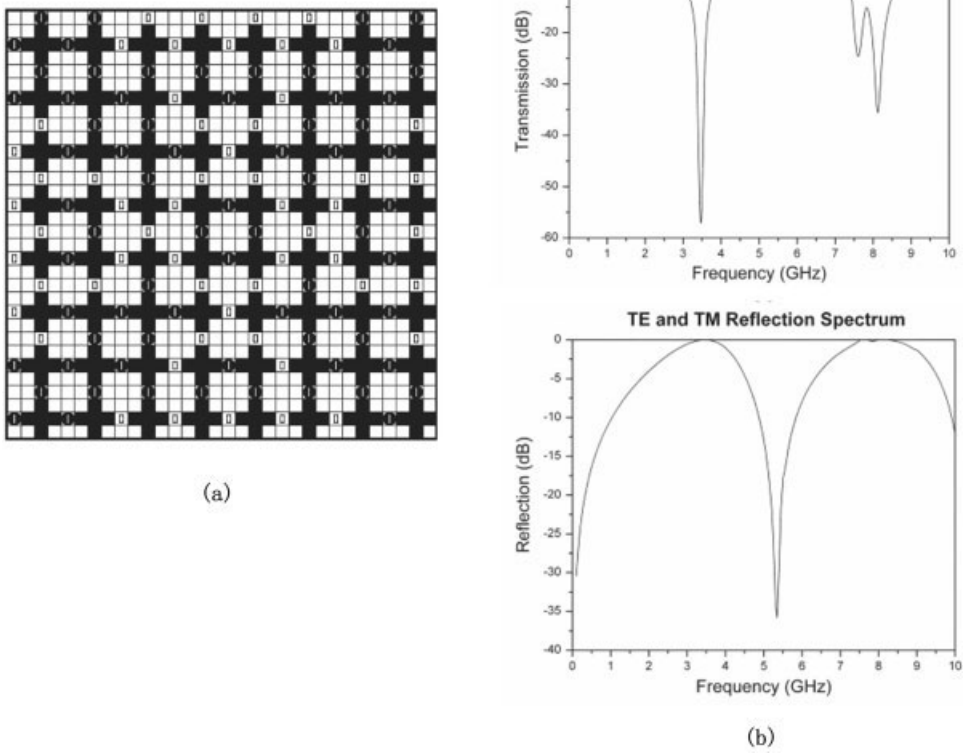

Figure 2 (a) A cross-dipole RFSS geometry with GA optimized switch settings "1 " indicates the switch is closed and a "0 " indicates the switch is open; (b) frequency response (transmission and reflection) for the FSS is shown in (a)

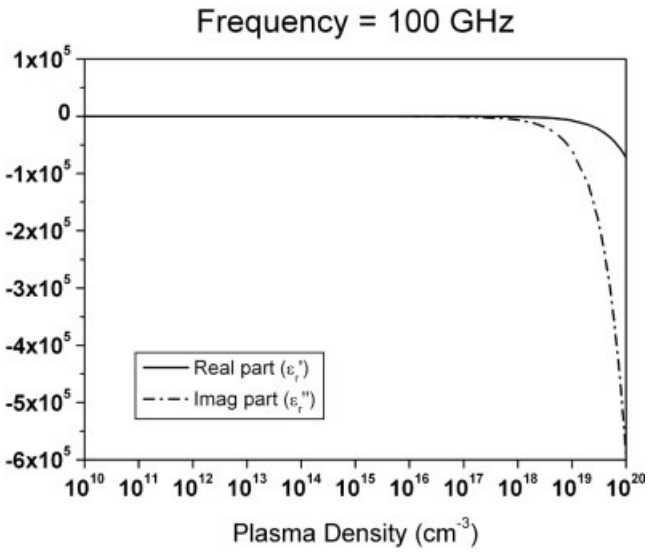

Figure 3 Calculated permittivity of silicon under varying photonic excitation

where n_{po} is the density of the intrinsic holes due to doping, n_p and n_e are the density of photo-induced holes and electrons, and the subscripts "p " and "e " refer to holes and electrons. The effective masses m^* and the lifetimes τ are related by

$$\tau_e = \frac{\mu_e m_e^*}{e}, \tag{3a}$$

$$\tau_p = \frac{\mu_h m_p^*}{e}. \tag{3b}$$

The numerical values that we use are: $m_0 = 9.1 \times 10^{-31}$ kg; $m_p^* = 0.38m_0$; $m_e^* = 0.259m_0$; $\tau_p = 1.3 \times 10^{-13}$ S; $\tau_e = 2.2 \times 10^{-13}$ S; $\mu_p = 600$ cm^2/V; $\mu_e = 1500$ cm^2/V and $n_{p0} = 10^{11}$ cm^3. We set $n_p = n_e$, which is the plasma density.

By controlling the plasma density inside the silicon through photonic illumination, one can realize a dramatic dynamic change in conductivity. Figure 3 shows the predicted variation of the real and imaginary parts of the permittivity ε_r of silicon at 100 GHz with plasma density. It can be seen that within the plasma density range shown, the change in the imaginary part of ε_r is more than five orders of magnitude, which indicates that silicon is a good switch material for use in a reconfigurable FSS design.

3. DESIGN CONCEPT

A proper design of a RFSS must take into account lossy FSS screen material transition properties. As discussed in the preceding section, silicon possesses a range of conductivities that depend on the intensities of laser light, which produces a plasma region. The extremes of this range can be considered the ON (highest conductivity) and OFF (lowest conductivity) states for the switches. A robust optimization tool based on the GA has been developed that

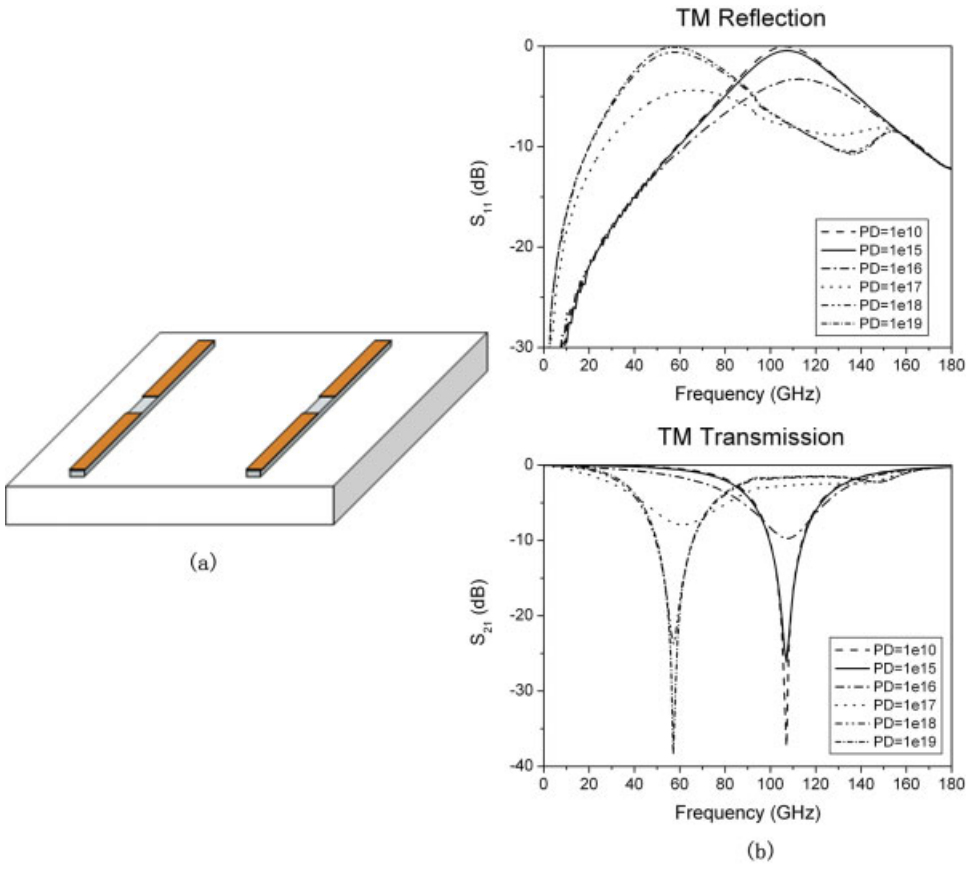

Figure 4 (a) Unit cell of metallodielectric RFSS with silicon switches; (b) frequency response (transmission and reflection) for the RFSS is shown in (a). [Color figure can be viewed in the online issue, which is available at www.interscience.wiley.com]

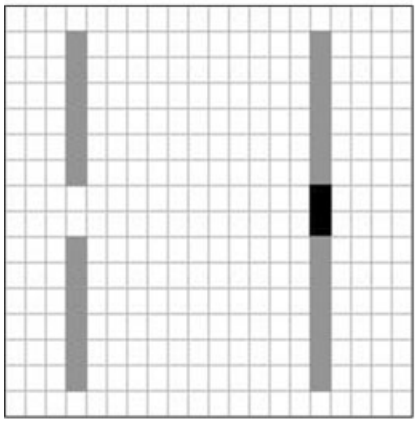

(a)

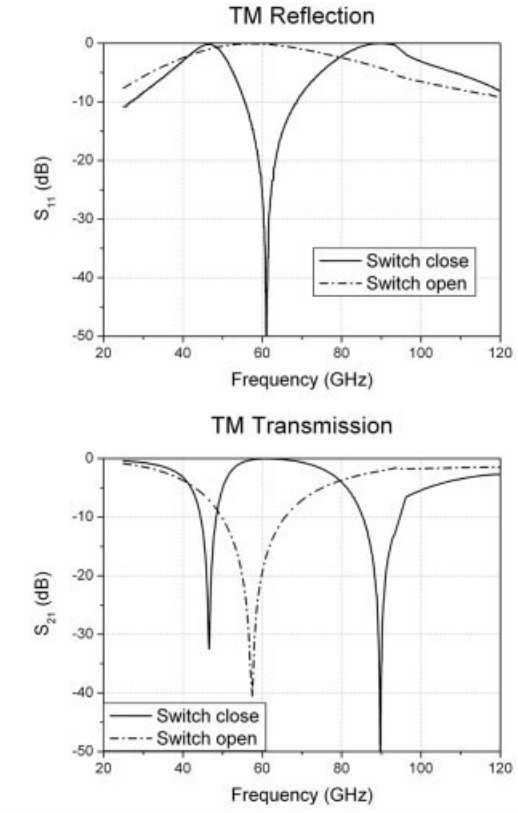

(b)

Figure 5 (a) Unit cell (black blocks indicate the switch is closed); (b) frequency response (transmission and reflection) for the RFSS is shown in (a)

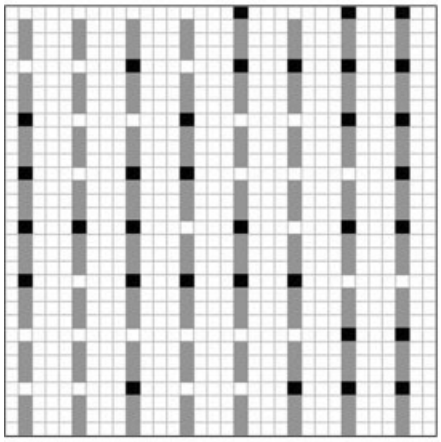

(a)

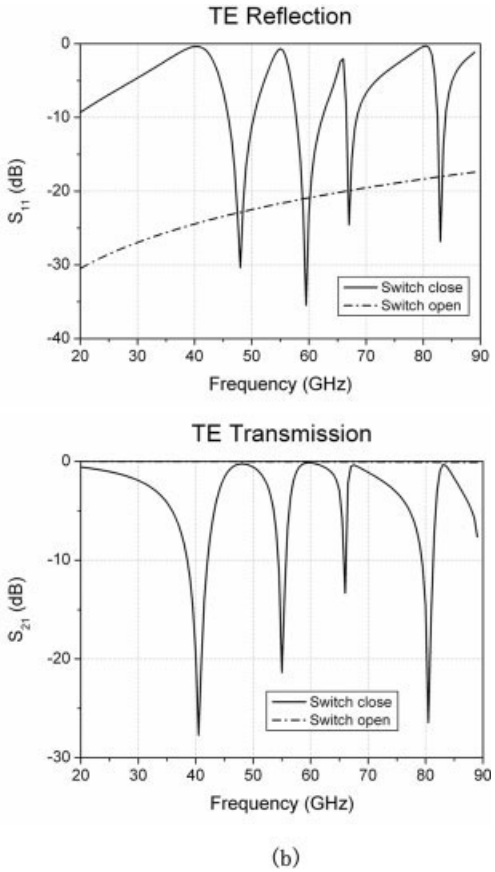

(b)

Figure 6 (a) GA optimized unit cell geometry (black blocks indicate the switch is closed); (b) frequency response (transmission and reflection) for the RFSS is shown in (a)

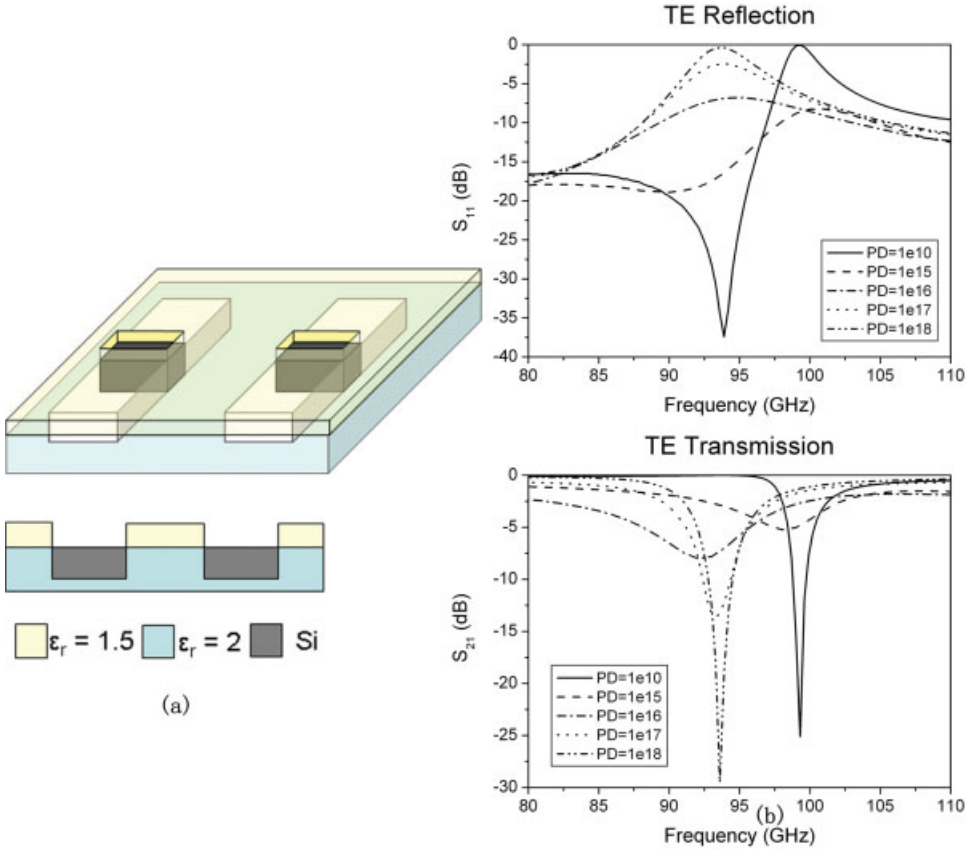

Figure 7 (a) Unit cell and cross section of an all-dielectric RFSS; (b) frequency response (transmission and reflection) for the RFSS shown in (a). [Color figure can be viewed in the online issue, which is available at www.interscience.wiley.com]

can effectively design reconfigurable FSS for the best possible performance. In the previous work [2], the GA has been shown to be a very powerful tool for designing RFSSs. For the designs considered in this article, a GA was used to optimize the switch locations (or settings), the size of the unit cell, the thickness of the substrate, and the permittivity of the substrate to generate the best ON and OFF state performances at desired operating frequencies. One can easily extend the methods introduced in this article to the design of multi-band RFSSs.

4. RESULTS

We first consider the response of a RFSS to incident plane waves of frequencies operating around 100 GHz. The RFSS is composed of a dielectric substrate with silicon strips as shown in Figure 4(a). Two metallic dipole patches are located on the surface of each silicon strip with a gap in between, which acts as a switch under photonic illumination. The size of the unit cell is 3.2 mm $\times$ 3.2 mm, and the thickness of the substrate is 0.04 mm. Each silicon strip is 2.8 mm $\times$ 0.2 mm $\times$ 0.01 mm and the perfectly conducting metallic patches are 1.2 mm $\times$ 0.2 mm. The dielectric constant of the substrate is chosen to be two. The response spectra of the RFSS are shown in Figure 4(b) over the expected range of plasma densities in silicon. As the plasma density increases from 10^{10} to 10^{19} cm^{-3}, the stopband in the transmission spectrum shifts from 110 to 60 GHz, demonstrating the reconfigurable behavior of the RFSS.

The second example shows a case of only one switch in each unit cell. When the switch is open, we obtained a stopband around 50 GHz, and when the switch is closed, we produced two stopbands at 50 and 90 GHz. All the other parameters are same as the previous example and the spectra are shown in Figure 5.

To obtain more flexibility and improved performance in our design of a RFSS, we then used the GA. In previous work [4] GAs have been shown to be an excellent means for optimizing the design of electromagnetic band gap type absorbers. Here, we used the GA to optimize the switch settings (i.e., which switches should be "ON" and which switches should be "OFF" to achieve a desired response). The size of the unit cell obtained is 3.2 mm $\times$ 3.2 mm, and the thickness of the substrate is 0.04 mm producing a structure similar to the two previous cases. But in this case, the unit cell screen is divided into 32 by 32 blocks [Fig. 6(a) for the screen geometry] and we let the GA pick out the switch locations to meet the preset requirements, which were four stopbands at 40, 55, 65, and 80 GHz. From Figure 6(b), one can see that we obtained four stopbands in the range from 20 to 90 GHz, thus illustrating the utility of the GA.

The fourth RFSS example utilized an all-dielectric design, using a substrate with two slots as illustrated in Figure 7(a). A silicon switch is placed in the middle of each slot, and a superstrate is placed on top with two holes at switch locations for the illumination control of the switch. The dimension of the unit cell is 2.2 mm $\times$ 2.2 mm $\times$ 1.98 mm. The substrate thickness is 1.32 mm, the slot size is 1.65 mm $\times$ 0.55 mm, and the silicon switch size is 0.55 mm $\times$ 0.275 mm $\times$ 0.88 mm. The thickness of the superstrate is 0.66 mm. The dielectric constant of the substrate and superstrate are chosen to be 2 and 1.5, respectively. The response spectra of the RFSS versus frequency are shown in Figure 7(b). Similar to the

first example, as the plasma density increases from 10^{10} to 10^{18} cm^{-3}, the stopband shifts from 100 to 93 GHz.

5. CONCLUSIONS

Signals at frequencies around 100 GHz (D-band) and above are of interest for several applications including atmospheric sensing, wideband communications, automotive radar, and test instrumentation. In this article we presented a new design concept for reconfigurable FSSs that uses silicon as a substrate for switches and applied it to two types of RFSS examples that operate at a target frequency of 100 GHz, the first type of design uses metallic patches and the second one utilizes all-dielectric materials. The designs proposed can be readily fabricated and are easily scaled to lower or higher frequencies. A robust GA technique was developed and successfully applied to evolve optimal designs for single-band and dual-band RFSSs.

REFERENCES

1. T.K. Wu, Frequency selective surface and grid array, Wiley, New York, 1995.
2. J.A. Bossard, D.H. Werner, T.S. Meyer, and R.P. Drupp, Proceedings of the 2004 IEEE antennas and propagation international symposium, II, Monterey, CA, (2004), 1911.
3. J.A. Bossard, D.H. Werner, T.S. Mayer, and R.P. Drupp, IEEE Trans Antennas Propag 53 (2005), 1390.
4. C. Lee, P. Mak, and A. DeFonzo, IEEE J Quantum Electron 16 (1980), 277.

NEW BALANCED UWB PLANAR ANTENNA

Y. X. Guo,[1] Y. F. Ruan,[1,2] Z. Y. Zhang,[1] L. C. Ong,[2] and X. Q. Shi[2]

[1] Institute for Infocomm Research
20 Science Park Road
No. 02–21/25, TeleTech Park
Science Park II, Singapore 117674
[2] Nanjing University of Science and Technology
200 Xiao Lingwei, Nanjing
Jiangsu 210094, China

Received 25 May 2006

ABSTRACT: *A new balanced planar ultra-wideband (UWB) antenna is proposed. First, a novel uniplanar broadband balun transition is presented. Then, a balanced UWB planar dipole antenna fed by the proposed balun is studied, and has a measured bandwidth from 2.8 to 11.2 GHz for the return loss better than −10 dB.* © 2006 Wiley Periodicals, Inc. Microwave Opt Technol Lett 49: 114–118, 2007; Published online in Wiley InterScience (www.interscience.wiley.com). DOI 10.1002/mop.22040

Key words: *balun; planar antennas; UWB antennas; balanced antennas*

1. INTRODUCTION

Ultra-wideband (UWB) antennas for wireless applications have received much attention recently [1–5]. Most of the proposed UWB antennas are based on planar monopole-like antennas. On the other hand, balanced UWB antennas are much of interest. A balanced-fed antenna features balanced operation, which leads to a significant reduction in the current induced on the ground plane, thus avoids such antenna performance degradation [6, 7]. A balun is one key component to realize such a balanced antenna.

A balun is a device for converting signals between an unbalanced circuit structure and a balanced circuit structure. The signal of a balanced circuit structure comprises two signal components with the same magnitude but 180° phase difference. Various types of baluns have been reported for applications in microstrip circuits, microwave integrated circuits (MICs), and monolithic microwave integrated circuits (MMICs). Among them, planar baluns are one of the most popular structures because of their ease of implementation and good performance. The planar baluns mainly consist of the simply half-wavelength line separation splitters, the multi-section half-wave baluns, and the coupled-line baluns [8]. The interface of the aforementioned baluns is mainly based on the same transmission line, e.g. microstrip line or CPW. On the other hand, one second category of balun can be referred to as a transition between an unbalanced line (microstrip or coplanar waveguide) and a balanced line such as broadside parallel strip and coplanar stripline (CPS). Broadside parallel stripline and CPS are both widely used in feeding networks of printed dipole antennas, balanced mixers, and optoelectronic circuits.

To date, a number of reported efforts have been dedicated to the bandwidth enhancement of balun transitions [9–14]. In Ref. 9, Dib et al. reported a type of microstrip-to-CPS transition based on the concept of mode conversion with a 3 dB back-to-back insertion loss bandwidth from 7 to 11.5 GHz. In Ref. 10, Qian and Itoh provided a microstrip-to-CPS transition from 6 to 13 GHz. Suh et al. presented a microstrip-to-CPS transition with an insertion loss of less than 3 dB and a return loss of better than 10 dB operating from 1.3 to 13.3 GHz in Ref. 11. For CPW-to-CPS transitions, many broadband transitions have also been developed. Tilley et al. [12] reported a wideband CPW-to-CPS transition with a 1 dB back-to-back insertion loss bandwidth from 0.45 to 5 GHz. Li et al. [13] proposed a CPW-to-CPS back-to-back transition with the bandwidth ranging from 0.4 to 3.6 GHz. Moreover, for microstrip-to-broadside parallel strip transitions, the planar form of the tapered balun structure proposed by Duncan and Minerva has demonstrated a very broadband performance [14]. Although many wideband planar baluns mentioned earlier have been studied, new wideband baluns are still of interest.

In this paper, a novel uniplanar broadband balun transition is presented, which can either be used as a microstrip-to-microstrip or a microstrip-to-CPS transition. The proposed balun transition consists of a section of asymmetrical tapered edge coupled transmission lines to increase its bandwidth. The performance of the newly proposed transition is investigated in terms of a microstrip-to-microstrip and a microstrip-to-CPS transition. Then, as an application example, a balanced UWB planar dipole antenna fed by the proposed planar tapered balun is studied.

2. PROPOSED PLANAR TAPERED BALUN

2.1 Geometry

The structure of the proposed balun transition is illustrated in Figure 1. The solid line is the outline of the metallization of the front side of the substrate while the back side is shaded. The proposed balun consists of a section of edge-coupled transmission lines. One of the coupled lines joins the input microstrip line and the other is connected with the ground plane through holes. The microstrip line at the input port is assumed to be 50 Ω. The main idea of this transition is to generate 180° difference at the output end of the coupled lines. Both of the conductors have a gradual taper in width to increase the bandwidth performance of the balun transition. To enhance the coupling and convert the electric field